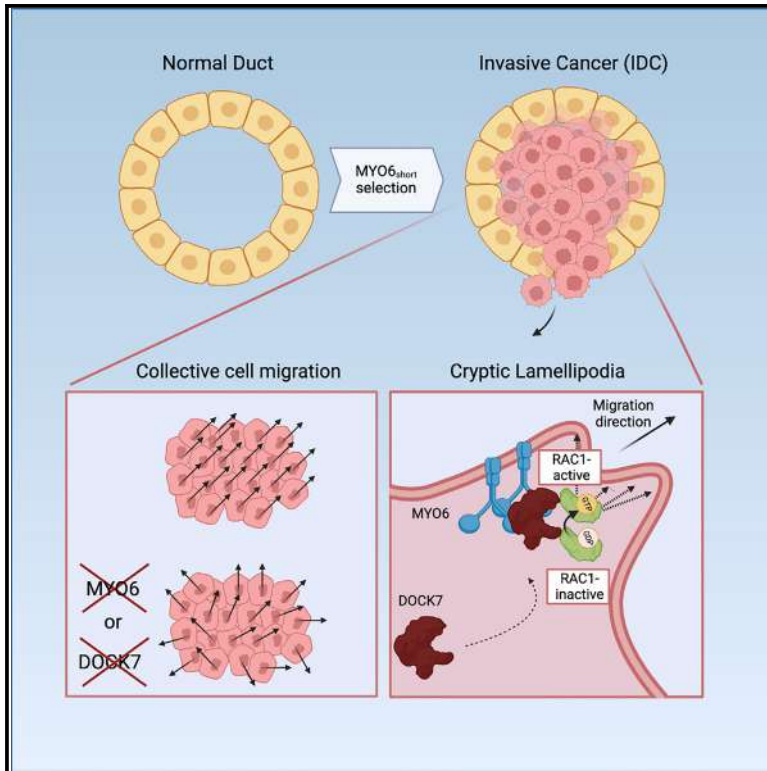# A planar polarized MYO6-DOCK7-RAC1 axis promotes tissue fluidification in mammary epithelia

Graphical abstract

Authors

Luca Menin, Janine Weber,
Stefano Villa, ..., Fabio Giavazzi,
Giorgio Scita, Simona Polo

Correspondence

giorgio.scita@ifom.eu (G.S.),
simona.polo@ifom.eu (S.P.)

In brief

Menin et al. reveal that the collective motion of jammed epithelia depends on a MYO6-DOCK7-RAC1 axis operating specifically in follower cells. Activation of this pathway promotes the orientation and persistence of cryptic lamellipodia, enabling long-range coordination of movements of epithelial cells during tissue fluidification, wound repair, and invasive outgrowth.

Highlights

- Collective motion of jammed epithelia requires myosin VI

- MYO6-DOCK7 axis is critical to restrict activity of RAC1 in a planar polarized fashion

- MYO6-DOCK7-RAC1 axis ensures long-range coordination of movements in follower cells

- Myosin VI short expression is elevated in infiltrating breast cancer cells

Article

A planar polarized MYO6-DOCK7-RAC1 axis promotes tissue fluidification in mammary epithelia

Luca Menin,[1,8] Janine Weber,[1,9] Stefano Villa,[2,10] Emanuele Martini,[1] Elena Maspero,[1] Carlos A. Niño,[1] Valeria Cancila,[3] Alessandro Poli,[1] Paolo Maiuri,[4] Andrea Palamidessi,[1] Emanuela Frittoli,[1] Fabrizio Bianchi,[5] Claudio Tripodo,[1,3] Kylie J. Walters,[6] Fabio Giavazzi,[2] Giorgio Scita,[1,7,*] and Simona Polo[1,7,11,*]

[1]IFOM ETS, The AIRC Institute of Molecular Oncology, Milan, Italy
[2]Dipartimento di Biotecnologie Mediche e Medicina Traslazionale, Università degli Studi di Milano, Segrate, Italy
[3]Human Pathology Section, Department of Health Sciences, University of Palermo School of Medicine, Palermo, Italy
[4]Department of Molecular Medicine and Medical Biotechnology, University of Naples Federico II, Naples, Italy
[5]Unit of Cancer Biomarkers, Fondazione IRCCS Casa Sollievo della Sofferenza, San Giovanni Rotondo, Italy
[6]Protein Processing Section, Center for Structural Biology, Center for Cancer Research, National Cancer Institute, National Institutes of Health, Frederick, MD 21702, USA
[7]Dipartimento di Oncologia ed Emato-oncologia, Università degli Studi di Milano, Milan, Italy
[8]Present address: Università degli Studi di Milano, Milan, Italy
[9]Present address: Human Technopole, Milan, Italy
[10]Present address: Max Planck Institute for Dynamics and Self-Organization, Göttingen, Germany
[11]Lead contact
*Correspondence: giorgio.scita@ifom.eu (G.S.), simona.polo@ifom.eu (S.P.)
https://doi.org/10.1016/j.celrep.2023.113001

SUMMARY

Tissue fluidification and collective motility are pivotal in regulating embryonic morphogenesis, wound healing, and tumor metastasis. These processes frequently require that each cell constituent of a tissue coordinates its migration activity and directed motion through the oriented extension of lamellipodium cell protrusions, promoted by RAC1 activity. While the upstream RAC1 regulators in individual migratory cells or leader cells during invasion or wound healing are well characterized, how RAC1 is controlled in follower cells remains unknown. Here, we identify a MYO6-DOCK7 axis essential for spatially restricting RAC1 activity in a planar polarized fashion in model tissue monolayers. The MYO6-DOCK7 axis specifically controls the extension of cryptic lamellipodia required to drive tissue fluidification and cooperative-mode motion in otherwise solid and static carcinoma cell collectives.

INTRODUCTION

Collective motility and tissue fluidification are emerging as key regulators in physiological tissue remodeling during development, wound repair, and regeneration and in pathological conditions, first and foremost during carcinoma dissemination.[1–5] During these processes, individual cells composing a given tissue coordinate their motion with that of their neighbor cells by keeping tight cell-cell contacts to migrate or invade.[6]

A remarkable form of collective dynamics occurs during the early development of epithelial and glandular tissues, which are characterized by individual cells that constantly rearrange their motion, as in a fluid. This fluid-like property endows tissues with a large degree of plasticity that is instrumental in the initial phases of tissue specification and morphogenesis. As density rises because of proliferation and tissues mature and differentiate, the motion of each cell is constrained by the crowding of its neighbors, forcing cells to move in groups in a highly coordinated and cooperative fashion.[7,8] At a critical density, motility ceases, and tissues rigidify to undergo a fluid-to-solid phase transition, a process recently referred to as a jamming transi-

tion.[9] This tissue-level phase transition has been proposed to be critical for development of the elastic properties and barrier function of epithelial tissues and might also act as an intrinsic homeostatic mechanical barrier to development and expansion of structurally altered, hyperdynamic oncogenic clones. Conversely, a certain degree of fluidity is needed for a tissue to repair a wound, proliferate, or locally disseminate, such as during carcinoma progression.[1,4]

Tissue fluidification and collective motility are ruled by biochemical and physical interactions cells establish with each other and their environment.[2,10] How cells and tissues regulate this process and control these parameters has only begun to be investigated. To drive and propel directed cell migration, cells need to dynamically reorganize their actin cytoskeleton and generate actively pushing lamellipodial cell protrusions.[11] When embedded in a fully confluent monolayer or a developing epithelial tissue, cell protrusions can no longer extend into free space but are forced to either push adjacent neighboring cells or slip underneath them and are commonly referred to as cryptic lamellipodia.[12] Coordinated and directed extension of cryptic lamellipodia along a common direction drives groups of cells
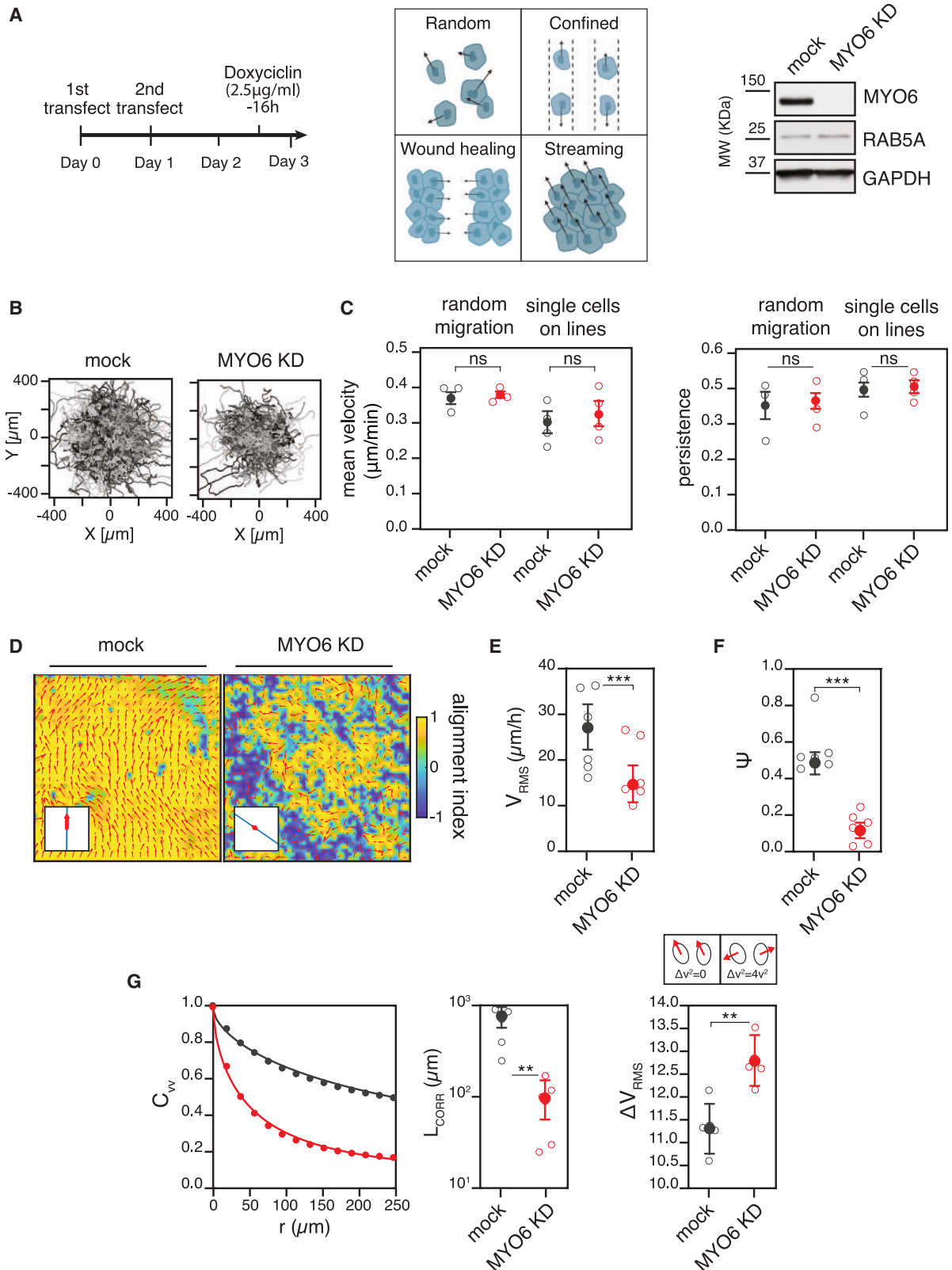
(legend on next page)

to move either as a solid rotating flock, such as in the case of the follicular epithelial cells in *Drosophila melanogaster*,[13] or as supracellular streams that fluidize the whole tissue, as during compression- or endocytosis-driven unjamming of human bronchial epithelial tissue and model mammary epithelial cells.[14,15]

We have shown previously that elevated levels of RAB5A, a master regulator of early endosomes, is sufficient to re-awaken the motility of otherwise kinetically arrested epithelial monolayers, promoting millimeter-scale flocking-fluid motility through large-scale coordinated migration and local cell rearrangements.[14,16–18] At the molecular level, RAB5A impinges on junction topology, turnover, and tension, fostering extension of oriented and coordinated cryptic lamellipodia.[14,17] The leading edges of cryptic lamellipodia, much like those of individual crawling cells, are generated by localized and spatially restricted actin polymerization triggered by numerous actin regulators and coordinated by the small GTPase RAC1.[14,19] However, the molecular machinery driving cryptic lamellipodium protrusion is likely to be distinct or enriched with specific components with respect to more canonical lamellipodia of cells moving individually or into free space. Indeed, a distinct cell identity with a leader-to-follower topological organization is emerging as critical in driving directed collective motion, such as in the case of Indian-file-moving cells,[20] protruding multicellular fingers extending into the free space during wound closure in model epithelia,[21] or cell-cohort-invading stromal tissues during carcinoma dissemination.[4,22,23]

Among the proteins that regulate cell migration and membrane protrusion, myosin VI is an unconventional actin-based motor protein that moves toward the minus end of actin filaments.[24–26] Myosin VI was originally characterized in *Drosophila melanogaster*, where it participates in collective migration of border cells during ovary development.[27,28] The pro-migratory function of myosin VI has also been confirmed in tumors, where elevated levels of this protein are frequent and correlate with the aggressive behavior in ovarian, breast, and prostate cancer.[26,28–31] In epithelial carcinoma, deregulated alternative splicing results in preferential or exclusive expression of the short isoform of myosin VI, to which a cancerous malignancy becomes addicted for migration.[31] Despite the increasing interest in the potential oncogenic role of myosin VI in cell migration, little is known about its mechanism of action and potential impact on cancer collective migration capacity.

Here, we employ oncogenic monolayer models in which RAB5A expression can be tuned in an inducible fashion to promote flocking-fluid motility and test the impact of myosin VI. We uncover a myosin VI-DOCK7 axis as critical for spatially restricting the activity of RAC1 in a planar polarized fashion. Myosin VI is specifically required in follower cells to promote formation of cryptic lamellipodia that drive tissue fluidification by triggering highly coordinated and cooperative-mode motion in otherwise solid and static carcinoma cell collectives.

RESULTS

### Myosin VI is critical for coherent motion of jammed epithelia

Myosin VI is required for cancer cell migration through an ill-defined molecular mechanism.[25,31] We examined the role of myosin VI during individual and collective cell migration; namely, during random and confined migration of single cells or in wound healing and tissue fluidification via flocking stream in epithelial monolayers (Figure 1A). To directly compare the results, we exploited the oncogenically transformed MCF10.DCIS.com cell line, in which collective streaming of cells in densely packed and confluent monolayers can be induced by modulation of RAB5A expression[14] (hereafter referred to as ductal in situ carcinoma [DCIS]-RAB5A). This cell line uniquely expresses the short isoform of myosin VI (Figure S1A) and, thus, represents the ideal model system to identify specific roles of this isoform.

Silencing of myosin VI with specific small interfering RNA (siRNA) oligos had no impact on the mean velocity or persistence of motility of individual cells in random or confined migration assays (Figures 1B and 1C; Videos S1 and S2). Conversely, in wound healing experiments, myosin VI depletion caused impairment of collective migration, consistent with previous findings.[31] The defective collective motion is the result of a reduction in the global velocity of wound closure (Figure S1B; Video S3), likely because of impairment of cell directionality (Figure S1C). A second siRNA myosin VI oligo showed similar depletion efficiency and almost identical results (Figures S1D and S1E).

We then analyzed the reawakening of collective migratory properties during unjamming of otherwise solid and static epithelial monolayers. Time-lapse image sequences of control and knockdown (KD) cells were analyzed by particle image velocimetry

Figure 1. Myosin VI is required for coherent motion of jammed epithelia

(A) Experimental pipeline used for all kinetics experiments using DCIS-RAB5A and derivative cell lines. Right: representative immunoblot (IB) analysis of the indicated lysates (day 3).

(B) Representative example of single-cell trajectories obtained from random migration assays with the indicated cell lines.

(C) Quantification of single cell motion assays with the indicated cell lines. n = 75 (25 single cells/experiment/genotype for three independent experiments). Empty circle, mean of the single experiment. Error bars, ±SD. not significant (ns) > 0.999 by Student's t test.

(D) Representative snapshots of the velocity field obtained by PIV analysis (red arrows), taken at 8 h after the beginning of the experiment. The color map represents the alignment with respect to the mean instantaneous velocity, quantified by the alignment index $a(x) = \boldsymbol{v}(x) \cdot \boldsymbol{v_0} / |\boldsymbol{v}(x) \cdot \boldsymbol{v_0}|$, which is equal to 1(−1) when the local velocity is parallel (antiparallel) to the mean direction of migration. Red arrows in each inset represent the mean velocity v_0 (average over the entire field of view).

(E) Root-mean-square velocity V_{RMS} parameter obtained from the PIV analysis of six independent experiments. Empty circle, mean of each experiment calculated from at least five videos/condition. Error bars, ±SD. ***p < 0.001 by Student's t test.

(F) Orientational order parameter ψ obtained from the PIV analysis described in (E). Error bars, ±SD. ***p < 0.001 by Student's t test.

(G) Left: velocity correlation functions $C_{vv}(r)$ obtained from PIV analysis (symbols) and best-fitting curves with a stretched exponential model (continuous lines). Center: correlation length L_{corr} obtained from the fitting procedure, the corresponding average stretching exponent β being 0.69 ± 0.07 and 0.76 ± 0.05 for mock and MYO6 KD, respectively. Error bars, ±SD. **p < 0.01 by Student's t test. Right: mean square relative velocity Δv_{RMS} of pairs of neighboring cells obtained from nuclear tracking.
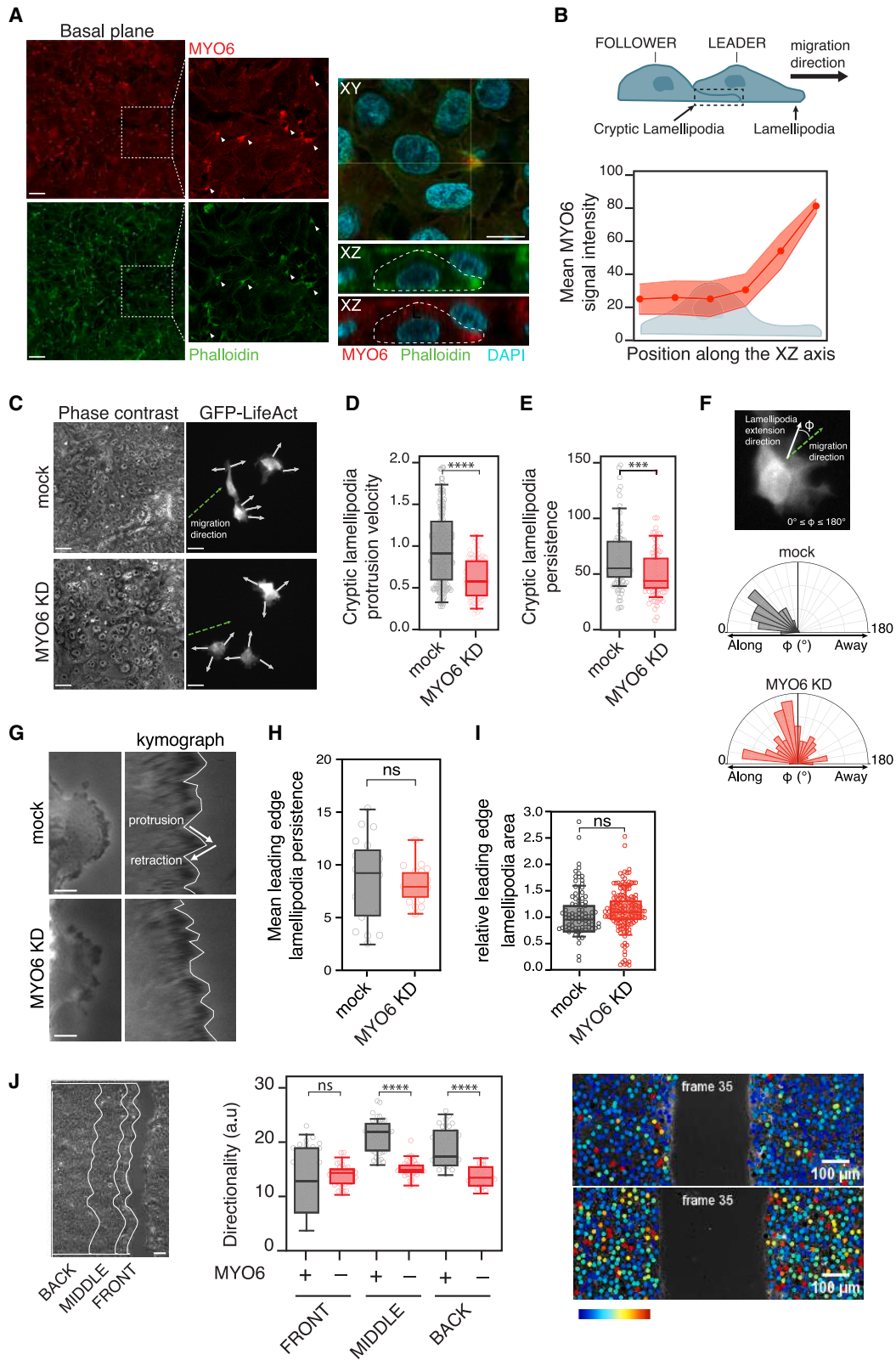
(PIV) to determine the local prevalent direction of motion and obtain time-resolved, coarse-grained velocity fields.[14] As shown in Figure 1D and Videos S4 and S5, myosin VI depletion strongly impacts collective migration by reducing the overall cellular motility, quantified by the root-mean-square velocity v_{RMS} (Figure 1E) and, even more strikingly, by severely impairing long-range cell-cell coordination. The degree of mutual alignment of cellular velocities is captured by the polar order parameter ψ, which can vary in the range of $[0,1]$, with $\psi = 1$ corresponding to a perfectly uniform velocity field and $\psi \simeq 0$ to a randomly oriented velocity field (see STAR Methods for details). While we measure $\psi \simeq 0.5$ for the control monolayer, clearly indicating the presence of directed collective migration, we observed a 4- to 5-fold decrease in ψ for the myosin VI KD condition (Figure 1F). We confirmed the lack of long-range coordination in KD monolayers by calculating the velocity correlation functions $C_{vv}(r)$ and the corresponding correlation lengths L_{corr} (Figure 1G). L_{corr}, which roughly corresponds to the characteristic linear size of a "pack" of coherently migrating cells, displays a striking 20-fold reduction in KD cells. Intriguingly, besides reducing large-scale coordination, myosin VI depletion also enhances small-scale velocity fluctuations, as can be seen by considering the mean squared relative velocity $\sqrt{(<\Delta v_{RMS}>)^2}$ of neighboring cell pairs, which displays a significant increase in KD monolayers (Figure 1G). Of note, all of these effects are not due to a cell division defect because similar numbers of cells were present in fully confluent mock and myosin VI-depleted monolayers (Figure S1F), and this collective locomotion is unperturbed by replication inhibition.[14]

Altogether, these results showed that the critical role of myosin VI in controlling multicellular streaming-like motility is an emergent property of confluent monolayers.

Myosin VI coordinates cryptic lamellipodium dynamics in follower cells

Myosin VI has been reported to be localized at adherens junctions and to interact with the cytoplasmic tail of E-cadherin.[32–34] In DCIS-RAB5 cells, myosin VI displays a diffuse cytoplasmic pattern in isolated, sparsely seeded cells but rapidly accumulates at desmosomes when a cluster of two or more cells is established (Figure S2A). In confluent monolayers, myosin VI was also present at the basal level, where it accumulated in actin-rich protrusions, called cryptic lamellipodia, which extend underneath the neighboring cells and display a planar polarized distribution[12,35] (Figures 2A and 2B). Importantly, by monitoring the dynamics of cells expressing EGFP-LifeAct interspersed with non-fluorescent cells, we found that myosin VI depletion did not impair formation of cryptic lamellipodia (Figure 2C; Video S6) but severely reduced their velocity (Figure 2D) and persistence (Figure 2E).

One striking feature of flocking-fluid locomotion in DCIS-RAB5A cells is their long-range, persistent, and ballistic motility. This trait is driven by formation of highly coordinated cryptic lamellipodia oriented in the direction of motion. Myosin VI depletion strongly impaired the alignment of these protrusions along the motility direction of supracellular motility streams (Figure 2F). Notably, myosin VI depletion specifically impaired cryptic lamellipodia in cell monolayers because its depletion did not alter the protrusion and persistence of lamellipodia generated in single cells (Figures S2B and S2C).

Cryptic lamellipodia are typically observed in follower cells during direct cell motility.[12] The streaming motility in monolayers, however, does not allow discernment of leader-to-follower topological cell organization. Thus, we analyzed myosin VI activity

Figure 2. Myosin VI coordinates cryptic lamellipodium dynamics in follower cells

(A) Basal plane of a fully confluent DCIS-RAB5A monolayer. Immunofluorescence (IF) analysis was performed as indicated. Arrows in the magnifications indicate the accumulation of myosin VI and phalloidin signals at the cryptic lamellipodia. Scale bars, 10 μm. Right panel: example of z stack projection of the same cells. Scale bars, 5 μm.

(B) Top: schematic of cryptic lamellipodium structure. Bottom: mean fluorescence signal of myosin VI across single cells from z stack acquisition images. n = 60 (4 independent experiments). Error bars, ±SD.

(C) Representative phase-contrast and fluorescence images of the streaming assay of mock or MYO6 KD monolayers where GFP-LifeAct-expressing cells were interspersed (1:10 ratio). Green arrow, direction of the migrating cell sheet. Scale bars, 15 μm.

(D) Quantification of cryptic lamellipodium protrusion velocity from the streaming assay described in (C). Results in the graph are expressed relative to GFP-LifeAct-expressing mock average value. The central mark indicates the median, and the bottom and top edges of the box indicate the 25th and 75th percentiles, respectively. An empty circle represents the mean lamellipodium protrusion velocity of a single cell. n = 145 (4 independent experiments). ****p < 0.0001 by Student's t test.

(E) Quantification of cryptic lamellipodium persistence from the streaming assay described in (C). Data are plotted as the number of frames in which the lamellipodium is detectable. An empty circle represents the persistence of single lamellipodia. n ≥ 74 (4 independent experiments). ***p < 0.001 by Student's t test.

(F) Top: representative image of the angle Φ between the direction of the cryptic lamellipodia (white arrow) and the direction of the migrating cell sheet (green arrow). Bottom plots: quantification of the orientation angle Φ for the indicated cell lines. n ≥ 140 (4 independent experiments).

(G) Representative phase-contrast images of leading-edge lamellipodia and their relative kymograph from scratched mock or MYO6 KD cell monolayers. Scale bars, 3 μm. Arrows in the kymograph highlight one protrusion and retraction event.

(H) Quantification of leading-edge lamellipodium persistence (expressed in minutes) obtained by kymograph analysis as in (G). An empty circle represents the persistence of single leading-edge lamellipodia. n = 20 (3 independent experiments). ns > 0.999 by Student's t test.

(I) Quantification of leading-edge lamellipodium mean area obtained by neural network[36] using phase-contrast images as in (G). Results in the graph are expressed relative to mock average value. An empty circle represents the area occupied by leading edge lamellipodia. n ≥ 80 (4 independent experiments). ns > 0.999 by Student's t test.

(J) Single-cell tracking of the wound healing assay performed on H2B-mCherry-expressing mock or MYO6 KD cells. Left: representative phase-contrast images of the wound healing assay. White lines define the area to which cells are assigned based on their distance from the wound edge. Scale bars, 50 μm. Center, quantification of the directionality of the cells belonging to the different area expressed as the inverse of the directional change rate parameter obtained with TrackMate. An empty circle represents the mean directionality of the tracks for each time-lapse video. n ≥ 30 (3 independent experiments). Error bars, ±SEM. ns > 0.999, ****p < 0.0001 by ANOVA. Right: visual representation of the tracking data quantified. Each nucleus is colored coded according to the direction persistence (from blue [high directionality] to red [low directionality]). One representative dataset is shown. Top: mock; bottom: MYO6 KD.
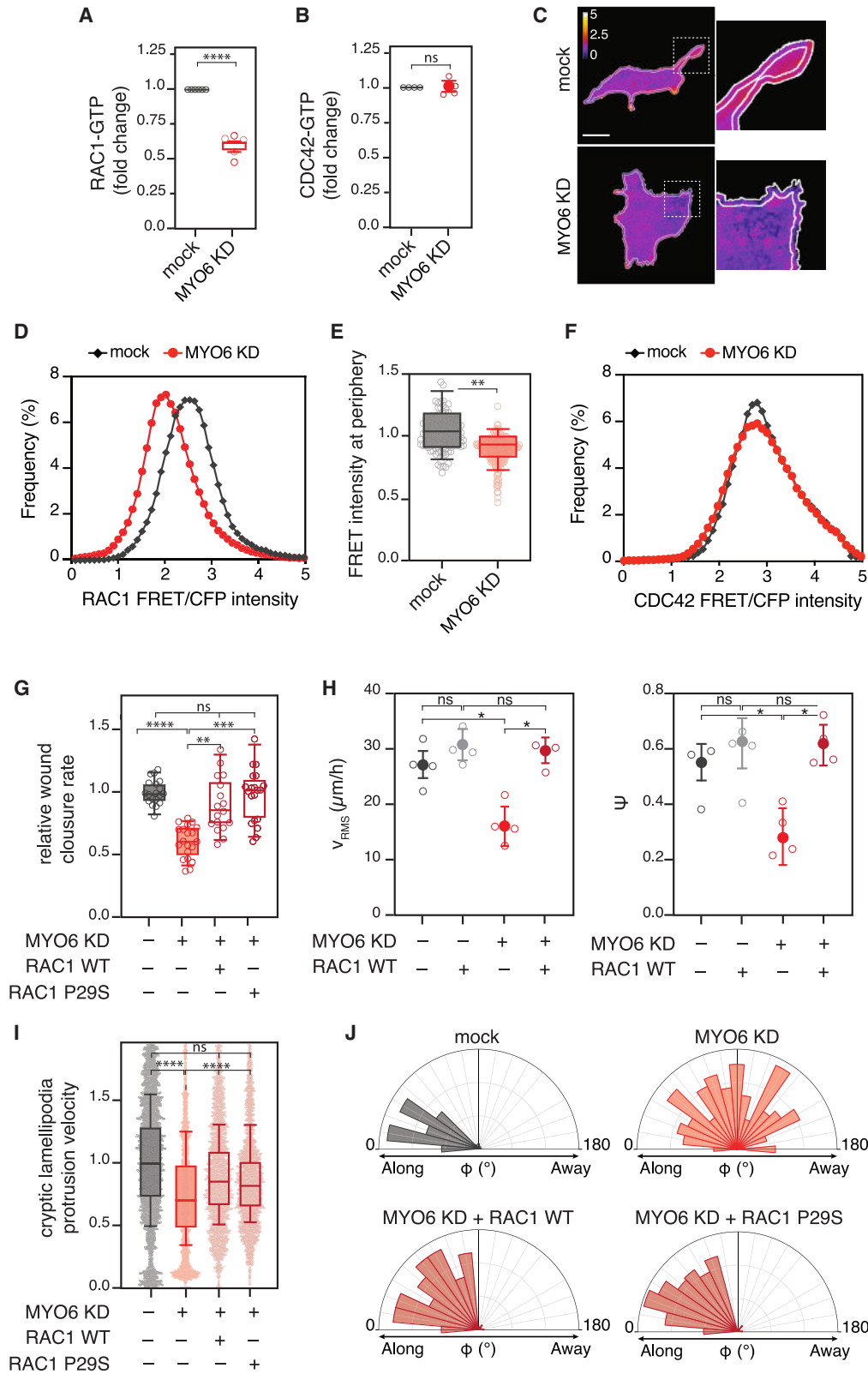
(legend on next page)

using a wound healing assay where the migratory phenotype caused by its depletion is evident (Figures S1B and S1C). For each cell, we measured its absolute speed and axial component in the direction of the wound by tracking its H2B-mCherry-labeled nucleus. Consistent with the specific role of myosin VI in the followers, silencing of the protein did not alter lamellipodium extension and persistence in leader cells at the wound front, as quantified by kymograph (Figures 2G and 2H) and neuronal network analyses[36] of the dynamics at the leading edges (Figure 2I). We also employed single-cell tracking analysis to evaluate the movement of cells located away from the wound edge. Strikingly, we found a significant reduction in cell directionality specifically in follower cells that were a few rows away from the wound edge (Figure 2J).

Collectively, these findings indicate that myosin VI specifically controls the coordinated persistence and dynamics of cryptic lamellipodia in follower cells, a prerequisite for collective movement.

Myosin VI regulates RAC1 GTPase activation at cryptic lamellipodia

A critical molecular determinant of cryptic lamellipodia is the small GTPases RAC1, whose activity is essential to trigger localized branched actin polymerization at the leading edge of migratory cells. We found that the total amount of active RAC1 was significantly reduced in myosin VI-depleted lysates from confluent cell monolayers (Figures 3A and S3A). Importantly, loss of myosin VI does not alter the level of active CDC42 (Figures 3B and S3B) or of RAC1 when lysates are prepared from isolated cells grown under sparse conditions (Figure S3C), reinforcing the notion of a specific function of myosin VI in controlling RAC1 activity in streaming, fluidized monolayers.

Next, we generated a stable DCIS-RAB5A cell line expressing a second-generation RAC1-fluorescence resonance energy transfer (FRET) biosensor.[37] Cells expressing the RAC1-FRET sensor were mosaically seeded in a confluent monolayer composed of non-fluorescent cells to enable measurement of RAC1 activation with high spatial resolution. In control cells, analysis of multiple protrusions revealed an increase in FRET ac-

tivity in proximity to the cell periphery (arbitrarily estimated at a distance of 1.5 µm from the plasma membrane), consistent with the established role of RAC1 activity in cryptic lamellipodia[38,39] (Figures 3C–3E). Strikingly, depletion of myosin VI significantly reduced the relative FRET signal of RAC1 activity in protrusions (Figures 3C–3E). Importantly, absence of myosin VI did not alter activation of CDC42, measured using a specific FRET biosensor[40] (Figure 3F). These results indicate that myosin VI is essential for optimal activation of RAC1 in cryptic lamellipodia that drive coordinated, long-range streaming motility.[35]

Finally, we tested whether constitutive activation of RAC1 was sufficient to rescue the phenotypes induced by myosin VI depletion using different orthogonal approaches. First, we found that addition of the cholinergic agonist and RAC1 activator carbachol[41,42] partially rescued the wound closure defect observed upon myosin VI depletion (Figure S3D). Next, we expressed wild-type (WT) RAC1) or its fast-cycling RAC1-P29S variant[43] in EGFP-LifeAct-expressing cells after silencing of myosin VI. WT RAC1 and RAC1-P29S were sufficient to rescue the wound closure defect (Figure 3G; Video S7) as well as the streaming defect observed in myosin VI-depleted cells upon RAB5A-induced unjamming. Indeed, ectopic expression of RAC1 in the cell monolayer was sufficient to rescue the loss of cell coordination measured by spatial velocity correlation lengths and root-mean-square velocity (Figure 3H; Video S8). Finally, we tested the dynamics of cryptic lamellipodia in the flocking, confluent monolayers. Expression of WT RAC1 or RAC1-P29S effectively restored the defective cryptic lamellipodium velocity (Figure 3I) and directional orientation (Figure 3J) caused by myosin VI depletion.

Altogether, these results demonstrate that myosin VI regulates localized activation of RAC1 specifically at cryptic lamellipodium protrusions to promote coordinated and collective cell migration and tissue fluidification.

Myosin VI controls RAC1 activation in cryptic lamellipodia by recruiting DOCK7

To gain insight into the molecular mechanisms underlying myosin VI regulation of RAC1 activity, we took advantage of the myosin VI

Figure 3. Myosin VI regulates RAC1 GTPase activation at cryptic lamellipodia

(A) GST-CRIB assay quantification from mock or MYO6 KD monolayers. Data are reported as fold change with respect to RAC1-GTP level in the corresponding mock sample for each experiment. n = 5 independent experiments. Reported values are mean ± SD. ****p < 0.0001 by Student's t test.

(B) As in (A) but for CDC42-GTP. Reported values are mean ± SD. ns > 0.999 by Student's t test.

(C) Representative images of RAC1-FRET biosensor-expressing mock or MYO6 KD cells. Scale bars, 10 µm. White lines define the area used for quantification of the FRET intensity signal at the cell periphery (<1.5 µm from the edge). The intensity, represented by a color scale, is shown. Right: magnification.

(D) Representative distribution of the normalized RAC1-FRET intensity signal at the cell periphery of a mock or MYO6 KD cell.

(E) Quantification of the FRET intensity signal at the cell periphery of mock or MYO6 KD cells. Results are expressed relative to mock average value. n ≥ 117 (4 independent experiments). **p < 0.01 by Student's t test.

(F) Representative distribution of the normalized CDC42-FRET intensity signal at the cell periphery of a mock or MYO6 KD cell.

(G) Wound healing assay results for the indicated cell lines. The average wound closure speed relative to the mock condition is plotted in the graph. The empty circle represents the mean wound closure velocity quantified for each video. n = 20 (4 independent experiments). ns > 0.999, **p < 0.01, ***p < 0.001, ****p < 0.0001 by ANOVA.

(H) PIV analysis of the streaming assay performed as in Figures 1E and 1F for the indicated cell lines. Left: root-mean-square velocity, V_{RMS}. Right: orientational order parameter, ψ. Empty circle, mean of the single experiment calculated from at least five videos/condition (four independent experiments). Error bars ±SD. ns > 0.999, *p < 0.05 by ANOVA.

(I) Quantification of cryptic lamellipodium protrusion velocity performed as in Figure 2D for the indicated cell lines. Results in the graph are expressed relative to GFP-LifeAct-expressing mock average value. An empty circle represents the mean lamellipodium protrusion velocity of a single cell. n = 144 (3 independent experiments). ns > 0.999, ****p < 0.0001 by ANOVA.

(J) Quantification of the orientation angle Φ performed as in Figure 2F. n = 132 for mock and MYO6 KD cells, n = 250 for MYO6 KD cells expressing wild-type (WT) RAC1 and RAC1-P29S (3 independent experiments).